ECCM21

02-05 July 2024 | **Nantes - France**

Proceedings of the 21st European Conference on Composite Materials

Vol 8

Special Sessions

WWW.ECCM21.ORG

UNDER THE PATRONAGE OF:

ESCM European Society For Composite Materials

Association pour les AMAC MAtériaux Composites

EuCIA The European Voice of Composites

WITH THE SUPPORT OF:

RÉGION PAYS DE LA LOIRE

ORGANIZED BY:

CENTRALE NANTES

Nantes Université

SUPPORTING PARTNER:

JEC CONNECTING THE WORLD WITH COMPOSITES

Edited by:

Prof. Christophe BINETRUY
ECCM21 Conference Chair
Institute of Civil Engineering and Mechanics (GeM)
Centrale Nantes
Nantes Université

Prof. Frédéric JACQUEMIN
ECCM21 Conference Co-Chair
Institute of Civil Engineering and Mechanics (GeM)
Nantes Université

Published by:

The European Society for Composite Materials (ESCM) and the Ecole Centrale de Nantes.

These Proceedings have an ISBN (owned by the Publisher) and a DOI (owned by the Ecole Centrale de Nantes).

ISBN: 978-2-912985-01-9
DOI: 10.60691/yj56-np80

Disclaimer:

CONTENTS

Editorial

Each volume gathers contributions on specific topics:

Vol 1. Industrial applications
Vol 2. Material science
Vol 3. Material and Structural Behavior – Simulation & Testing
Vol 4. Experimental techniques
Vol 5. Manufacturing
Vol 6. Multifunctional and smart composites
Vol 7. Life cycle performance
Vol 8. Special Sessions

This collection contains the proceedings of the 21st European Conference on Composite Materials (ECCM21), held in Nantes, France, July 2-5, 2024. ECCM21 is the 21st in a series of conferences organized every two years by the members of the European Society of Composite Materials (ESCM). As some of the papers in this collection show, this conference reaches far beyond the borders of Europe.

The ECCM21 conference was organized by the Nantes Université and the Ecole Centrale de Nantes, with the support of the Research Institute in Civil and Mechanical Engineering (GeM).

Nantes, the birthplace of the novelist Jules Verne, is at the heart of this edition, as are the imagination and vision that accompany the development of composite materials. They are embodied in the work of numerous participants from the academic world, but also of the many industrialists who are making a major contribution to the development of composite materials. Industry is well represented, reflecting the strong presence of composites in many application areas.

With a total of 1,064 oral and poster presentations and over 1,300 participants, the 4-day event enabled fruitful exchanges on all aspects of composites. The topics that traditionally attracted the most contributions were fracture and damage, multiscale modeling, durability, aging, process modeling and simulation and additive manufacturing.

However, the issues of energy and environmental transition, and more generally the sustainability of composite solutions, logically appear in this issue as important contextual elements guiding the work being carried out. This includes bio-sourced composites, material recycling and reuse of parts, the environmental impact of solutions, etc.

We appreciated the high level of research presented at the conference and the quality of the submissions, some of which are included in this collection. We hope that all those interested in the progress of European composites research in 2024 will find in this publication sources of inspiration and answers to their questions.

Prof. Christophe BINETRUY
ECCM21 Conference Chair
Institute of Civil Engineering
and Mechanics (GeM)
Centrale Nantes
Nantes Université

Prof. Frédéric JACQUEMIN
ECCM21 Conference Co-Chair
Institute of Civil Engineering
and Mechanics (GeM)
Nantes Université

CONTENTS

Under the Patronage of:

ESCM European Society For Composite Materials

Association pour les AMAC MAtériaux Composites

EuCIA The European Voice of Composites

Organized by: CENTRALE NANTES — Nantes Université

With the support of: RÉGION PAYS DE LA LOIRE

Supported by: EMC2 — JEC CONNECTING THE WORLD WITH COMPOSITES

Sponsored by:

Bronze Partner: BRUKER — INSTRON® — MatchID Metrology beyond colors

Other partners: CAPACITÉS De la recherche à l'innovation — CARBON AXIS — CETIM

Depestele — EikoSim — ELSEVIER — [redacted]

metravib material testing — NOVITOM — Quantiflex simulations — Surface Measurement Systems World Leader in Sorption Science

Hosting Organizations

Conference chairs

Prof. Christophe BINETRUY
ECCM21 Conference Chair
Institute of Civil Engineering and Mechanics (GeM)
Centrale Nantes
Nantes Université

Prof. Frédéric JACQUEMIN
ECCM21 Conference Co-Chair
Institute of Civil Engineering and Mechanics (GeM)
Nantes Université

International Scientific Committee

Malin Akermo (Sweden)
Remko Akkerman (Netherlands)
Andrey Aniskevich (Latvia)
Leif Asp (Sweden)
Emmanuel Baranger (France)
Janice Barton (UK)
Johnny Beaugrand (France)
Andrea Bernasconi (Italy)
Christophe Binetruy (France)
Thomas Bohlke (Germany)
Alain Bourmaud (France)
Nicolas Boyard (France)
Joël Breard (France)
Richard Butler (UK)
Baris Caglar (Netherlands)
Pedro Camanho (Portugal)
Pierpaolo Carlone (Italy)
Paolo Andrea Carraro (Italy)
Valter Carvelli (Italy)
Nuno Correia (Portugal)
Gergely Czél (Hungary)
Clemens Dransfeld (Netherlands)
Sylvain Drapier (France)
Klaus DRECHSLER (Germany)
Andreas ECHTERMEYER (Norway)
Paolo Ermanni (Switzerland)
Martin Fagerström (Sweden)
Ewald Fauster (Austria)
Julien Ferec (France)
Antonio Ferreira (Portugal)
Bodo Fiedler (Germany)
Stefanos Giannis (UK)
Nathalie Godin (France)
Carlos Gonzalez (Spain)
Sotirios Grammatikos (Norway)
Christoph Greb (Germany)
Emile Greenhalgh (UK)
Gianmarco Griffini (Italy)
Stephen Hallett (UK)
Nahiene Hamila (France)
Roland Hinterhoelzl (Austria)
Martin Hirsekorn (France)
Darko Ivančević (Hungary)
Frédéric Jacquemin (France)
Mikko Kanerva (Finland)
Luise Karger (Germany)
Vassilis Kostopoulos (Greece)
Theodosia Kourkoutsaki (Germany)
Thomas Kruse (Germany)
Ugo Lafont (France)
Jacques Lamon (France)
Frédéric Laurin (France)
Antoine Le Duigou (France)
Stepan Lomov (Belgium)
Theodoros Loutas (Greece)
Staffan Lundstrom (Sweden)
António Marques (Portugal)
David May (Germany)
Véronique Michaud (Switzerland)
Jörg Mussig (Germany)
Thomas Neumeyer (Germany)
Philippe Olivier (France)
Alkiviadis Paipetis (Greece)
Federico Paris (Spain)
Chung Hae Park (France)
John-Alan Pascoe (Netherlands)
Alessandro Pegoretti (Italy)
Ton Peijs (UK)
Rob Pierce (Denmark)
Soraia Pimenta (UK)
Silvestre Pinho (UK)
Gerald Pinter (Austria)
Connie Qian (UK)
Marino Quaresimin (Italy)
Andrew Rhead (UK)
Paul Robinson (UK)
Essi Sarlin (Finland)
Yentl Swolfs (Belgium)
Sofia Teixeira du Freitas (Netherlands)
Julie Teuwen (Netherlands)
Ole Thomsen (UK)
Stavros Tsantzalis (Greece)
Konstantinos Tserpes (Greece)
Albert Turon (Spain)
Julien van Campen (Netherlands)
Wim Van Paepegem (Belgium)
Anastasios Vassilopoulos (Switzerland)
Ignaas Verpoest (Belgium)
Michael Wisnom (UK)
Dimitrios Zarouchas (Netherlands)
Daiva Zeleniakiene (Lithuania)
Dan Zenkert (Sweden)

Local Organizing Committee

Suresh Advani
Romain Agogué
Sylvain Chataigner
Sébastien Comas-Cardona
Sofiane Guessasma
Suzanne Laïk
Philippe Le Bot
Mael Peron
Luisa Silva
Vincent Sobodka
Alexandre Ripoche
Elena Syerko

Table of Contents

Click on **CONTENTS** on the right side to return to the table of contents

Table of Contents

Table of Contents

Table of Contents

Table of Contents

Table of Contents

Table of Contents

Table of Contents

Table of Contents

Table of Contents

Table of Contents

Table of Contents

Table of Contents

Table of Contents

INVERSE COMPUTATION OF LOCAL FIBER ORIENTATION USING DIGITAL IMAGE CORRELATION AND DIFFERENTIABLE FINITE ELEMENT COMPUTATIONS

Nils Meyer[1] and Stefan Panzer[2]

[1]Data-driven Product Engineering and Design, Institute of Materials Resource Management, University of Augsburg, Am Technologiezentrum 8, 86159 Augburg, Germany
Email: nils.meyer@uni-a.de, Web Page: https://uni-augsburg.de/en/fakultaet/mntf/mrm/prof/ddped/
[2]Blackwave GmbH, Rotwandweg 8, 82024 Taufkirchen, Germany
Email: panzer@blackwave.de, Web Page: https://blackwave.de

Keywords: Injection Molding, Compression Molding, Differentiable Simulation

Abstract
Injection molding and compression molding are cost-effective processes for manufacturing discontinuous fiber reinforced polymer composite parts with complex geometries. The resulting properties of such parts depend on local fiber orientations, and we propose a novel approach to determine the orientation field as solution to an inverse problem: Given the deformation field of a part measured via digital image correlation (DIC), we determine the local orientations leading to that deformation. We model the structural deformation of the part with a differentiable finite element solver and mean field homogenization. Subsequently, we compute the error to the DIC measurement and minimize that error with respect to the input orientations. The gradients for optimization of the finite element model are computed efficiently using automatic differentiation with PyTorch through the entire model. The method is validated and discussed for carbon fiber sheet molding compounds under tensile loading but can be extended to arbitrary parts with defined load cases and available DIC data.

1. Introduction
Manufacturing of discontinuous fiber reinforced composites results in local variation of material orientation and properties. The local fiber orientation state is commonly described by second order fiber orientation tensors

$$\boldsymbol{A} = \int_{\mathcal{S}} \psi(\boldsymbol{p})\boldsymbol{p} \otimes \boldsymbol{p} \, \mathrm{d}A, \tag{1}$$

where $\boldsymbol{p}$ is a fiber direction and $\int_{\mathcal{S}} \mathrm{d}A$ describes integration over the surface of a unit sphere [1].
The orientation state may be computed with evolution equations for the orientation tensor or direct mechanistic models [2,3]. Such process simulations are time consuming, require extensive calibration of material models and may feature inaccuracies due to modeling assumptions. Consequently, there is a need to validate fiber orientation states by experimental techniques. One experimental method is X-Ray computer tomography (µCT) in combination with computational image processing based on structure tensors [4]. However, µCT scans are time consuming, require expensive equipment and are difficult to perform if the phase contrast is low, e.g. in carbon fiber polymer composites. Another experimental method is the image analysis of micrographs, where ellipsoid fiber cross sections are measured to estimate fiber orientations [5]. This image analysis of micrographs requires labor-intensive destructive specimen preparation and uses assumptions about the cross section of fibers. Both experimental methods are typically confined to specific regions of interest within a specimen and determination of a full orientation field for an entire component remains a challenge. We propose to formulate the problem of finding the orientation field as inverse problem, i.e. given a measured elastic deformation field, we want to determine the orientation field leading to that deformation.

CONTENTS

2. Methods

We subject a sample geometry to a tensile load and measure its surface deformation from both sides with DIC systems to gather as much deformation data as possible. Subsequently, we utilize a differentiable finite element model to minimize the error between simulation and measurement with respect to fiber orientations.

2.1. Experimental

For carbon fiber sheet molding compounds (CF-SMC), simple tensile specimens are often not feasible to evaluate the mechanical performance after molding, as they feature non-representative flow states. Therefore, Blackwave GmbH developed an SMC specimen with different thicknesses, radii, and ribs, which can be tested in universal tensile testing machines. A top view of this sample design is shown in Figure 1. Samples are manufactured with an Epoxy CF-SMC from *Mitsubishi Chemical Carbon Fiber and Composites, Inc.* with 58 wt.% fibers. We use two different initial stack placements covering 50% and 80% of the projected cavity area, respectively.

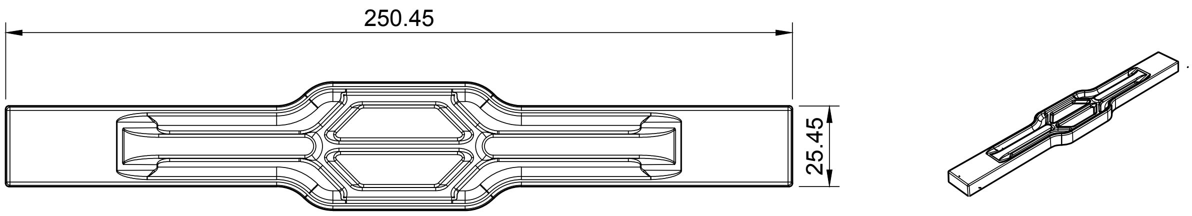

Figure 1. Specimen design. The dimensions (in mm) are adjusted to optical measurements such that they represent the actual manufactured shape accurately.

The specimens are clamped into a *ZwickRoell Kappa 050 DS* universal testing machine with a *ZwickRoell Xforce K* 50 kN load cell and subjected consecutively to 5 kN, 10 kN, 15 kN, and 20 kN with unloading after each step. The unloading allows us to determine whether the specimen has suffered inelastic damage, as we are interested only in the elastic deformation for the computational evaluation. Both the loading and unloading speed are 2 mm/min. Finally, we load the specimen with 5 mm/min until fracture. The deformation field is tracked at 2 Hz with two stereo DIC systems by *GOM Metrology*, as visualized in Figure 2.

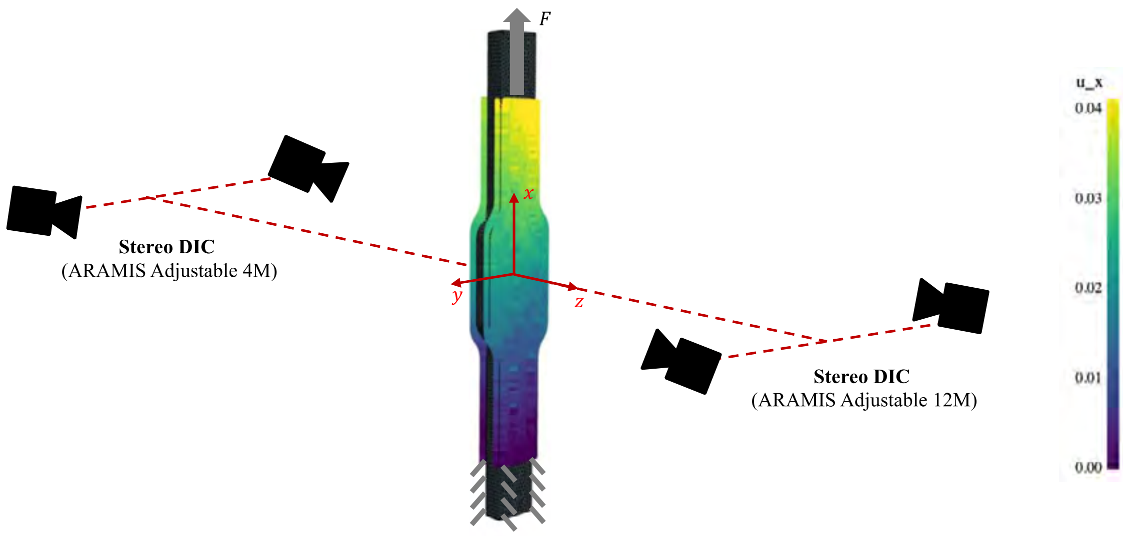

Figure 2. Setup for DIC measurement. Both point clouds and the mesh are transformed to a common global coordinate system and point colors indicate processed displacements in x-direction.

CONTENTS

We process raw data of facet positions by a rigid body transformation to a common coordinate system of a computational mesh (indicated in red in Figure 2), remove approximately 10 % of outlier points by filtering out displacement peaks with a prominence over 0.02 via *SciPy*, and compute a relative displacement field by subtracting the displacement of the lower clamping mechanism.

2.2. Computational

The displacement field $\boldsymbol{u}(\boldsymbol{x})$ is a solution to the anisotropic linear elastic boundary problem

$$\begin{aligned} \operatorname{div}(\boldsymbol{\sigma}) &= 0 \quad \boldsymbol{x} \in \Omega \\ \boldsymbol{u} &= \boldsymbol{u}_0 \quad \boldsymbol{x} \in \Gamma_{\mathrm{D}} \\ \boldsymbol{\sigma} \cdot \boldsymbol{n} &= \boldsymbol{t}_0 \quad \boldsymbol{x} \in \Gamma_{\mathrm{N}} \end{aligned} \tag{2}$$

on the computational domain of the specimen $\boldsymbol{\Omega}$ with Dirichlet boundary conditions at $\boldsymbol{\Gamma_{\mathrm{D}}}$ and Neumann boundary conditions at $\boldsymbol{\Gamma_{\mathrm{N}}}$ with boundary normal $\boldsymbol{n}$. The Dirichlet boundary conditions constrain all degrees of freedom at the bottom clamping and all except for displacement in x-direction at the top clamping. The Neumann boundary is a vertical force applied to the top clamping region such that it resembles the net force applied during the experiment. The stress tensor $\boldsymbol{\sigma}$ is related to the infinitesimal strain tensor $\boldsymbol{\varepsilon}$ via an anisotropic stiffness tensor $\mathbb{C}(\boldsymbol{A})$ as

$$\boldsymbol{\sigma} = \mathbb{C}(\boldsymbol{A}) : \boldsymbol{\varepsilon}. \tag{3}$$

The stiffness tensor depends on the local fiber orientation tensor and is obtained via volume averaging [1] of a unidirectional composite stiffness tensor, where we employ an IBOF closure for the fourth order fiber orientation tensor [6]. The unidirectional composite stiffness tensor is computed via a Mori-Tanaka mean field homogenization for isotropic materials with the aspect ratio of a fiber bundle a and fiber volume fraction v_{F} [7]. The material parameters are summarized in Table 1. Evaluating the homogenization method and orientation averaging for a quasi-planar fiber orientation state $\boldsymbol{A} = \operatorname{diag}(0.48, 0.48, 0.04)$ results in a planar elastic modulus of 36.6 GPa, which agrees with the manufacturer datasheet and thus verifies the homogenization procedure.

Table 1. Material parameters for elastic homogenization.

Property	E_{Matrix}	E_{Fiber}	ν_{Matrix}	ν_{Fiber}	v_f	a
Unit	GPa	GPa	-	-	%	-
Value	4.45	235.0	0.37	0.27	46.6	34

The linear elastic boundary problem (2) is solved numerically with the differentiable finite element solver *torch-fem* [8]. The numerical solution uses $M = 85{,}279$ tetragonal elements with linear shape functions to discretize the domain and solves for nodal displacements $\boldsymbol{u}_i(\mathcal{A})$ at each node i. The computed displacements depend on the tuple of element-wise orientation states $\mathcal{A} = (\boldsymbol{A}^1, \boldsymbol{A}^2, \dots, \boldsymbol{A}^M)$. The fundamental idea of this work is now the formulation of a loss term that quantifies the difference between observed displacements and computed displacements. Subsequently we minimize the loss with respect to fiber orientations in the computational model to yield an orientation state that causes the observed displacement. To do so, the fiber orientation in each element $j \in [1, M]$ is parametrized by its first two eigenvalues e_1^j and e_2^j as well as three orientation angles $\alpha^j, \beta^j, \gamma^j$, which describe an intrinsic rotation about axes z, y, x, respectively. In contrast to a parametrization by components, this ensures conservation of the tensor properties, and we can reconstruct the second order orientation tensors via

$$\boldsymbol{A}^j = \boldsymbol{R} \boldsymbol{A}_0^j \boldsymbol{R}^\top \tag{4}$$

with a rotation matrix $\boldsymbol{R}$ depending on $\alpha^j, \beta^j, \gamma^j$ and $\boldsymbol{A}_0^j = \operatorname{diag}(e_1^j, e_2^j, 1 - e_1^j - e_2^j)$. To ensure mesh independency, we filter the variables according to

$$\hat{\zeta}^j = \frac{\sum_i H_{ij}\zeta^i}{\sum_i H_{ij}} \qquad \zeta \in \{e_1, e_2, \alpha, \beta, \gamma\} \tag{5}$$

with a filter matrix

$$H_{ij} = \begin{cases} R - \operatorname{dist}(i,j), & \text{if } \operatorname{dist}(i,j) \leq R \\ 0, & \text{else} \end{cases} \tag{5}$$

where R describes the filter radius and $\operatorname{dist}(i,j)$ computes the distance between element centers i and j. The filter matrix is sparse and can be pre-computed once for a mesh and radius. The radius is a measure for the length scale at which orientation states change within the specimen independently of mesh size. To formulate the loss, we interpolate the nodal displacement vectors $\boldsymbol{u}_i(\mathcal{A})$ of the computational mesh to the DIC facet locations $\boldsymbol{x}_k \in \mathbb{R}^3$ in the undeformed state. This results in N pairs of observed displacement vectors $\boldsymbol{u}_k \in \mathbb{R}^3$ and interpolated displacement solutions $\widetilde{\boldsymbol{u}}_k(\mathcal{A}) \in \mathbb{R}^3$, which we use to formulate the loss as

$$\mathcal{L}(\mathcal{A}) = \sqrt{\sum_{k=1}^{N} \|\widetilde{\boldsymbol{u}}_k(\mathcal{A}) - \boldsymbol{u}_k\|_2^2}, \tag{6}$$

where $\|\cdot\|_2^2$ denotes the squared L^2 norm. Now, we want to solve the optimization task

$$\begin{aligned} &\min_{\mathcal{A}} \mathcal{L}(\mathcal{A}) \\ \text{s.t. } &\frac{1}{3} < \hat{e}_1^j < 1 \\ &\frac{1}{2}\left(1 - \hat{e}_1^j\right) < \hat{e}_2^j < \min\left(\hat{e}_1^j, 1 - \hat{e}_1^j\right), \end{aligned} \tag{7}$$

where the limits ensure feasible orientation states [9]. The optimization is performed with an ADAM optimizer in *PyTorch* using automatic differentiation with respect to $\boldsymbol{\mathcal{A}}$, which is expressed by the parametrization $e_1^j, e_2^j, \alpha^j, \beta^j, \gamma^j$. The initial state is planar isotropic in the x-y plane with uniform random noise between -5° and 5° in the orientation angles. We account for the constraints by gradient projection, i.e. we clamp each update to the feasible variable range. A simple forward evaluation of displacements takes ~10s and a full iteration of the optimizer including backward pass takes ~25s with double precision on an *Apple M1 Pro* CPU.

3. Results and discussion

We tested five specimens with 50% mold coverage and three specimens with 80% mold coverage. The experimental results are summarized in Table 2.

The stiffness and net force for simulations are evaluated in the linear elastic regime at the very beginning of the test between load step 3 and load step 10, where the specimen is slightly stretched but far from experiencing inelastic damage. We consider only this elastic deformation for the inverse method but report maximum force until fracture for completeness.

Table 2. Tested specimen data.

Identifier	Mold coverage	Stiffness	Sim. Force	Max. Force
24	50 %	33.4 kN/mm	1348 N	13.7kN
25	50 %	40.9 kN/mm	1022 N	17.9 kN
26	50 %	37.6 kN/mm	1417 N	21.3 kN
30	50 %	37.1 kN/mm	1684 N	32.6 kN
33	50 %	36.8 kN/mm	1242 N	15.5 kN
28	80 %	23.6 kN/mm	902 N	14.0 kN
31	80 %	25.3 kN/mm	1047 N	13.2 kN
32	80 %	25.0 kN/mm	1088 N	9.6 kN

There is a significant difference in the linear elastic stiffness between specimens with 50% mold coverage (37.16±2.67 kN/mm) and specimens with 80% mold coverage (24.63±0.91 kN/mm). This is expected, as lower mold coverage promotes a higher fiber orientation into the flow direction which in turn increases the stiffness in x-direction.

Figure 3 shows exemplary displacements of Specimen 31 measured with both DIC systems after filtering. We picked this specimen randomly to illustrate some results in more detail – others are qualitatively the same but reporting all of them would simply go beyond the scope of this article. The 12M system tends to capture finer local variations, but both systems are in reasonable agreement.

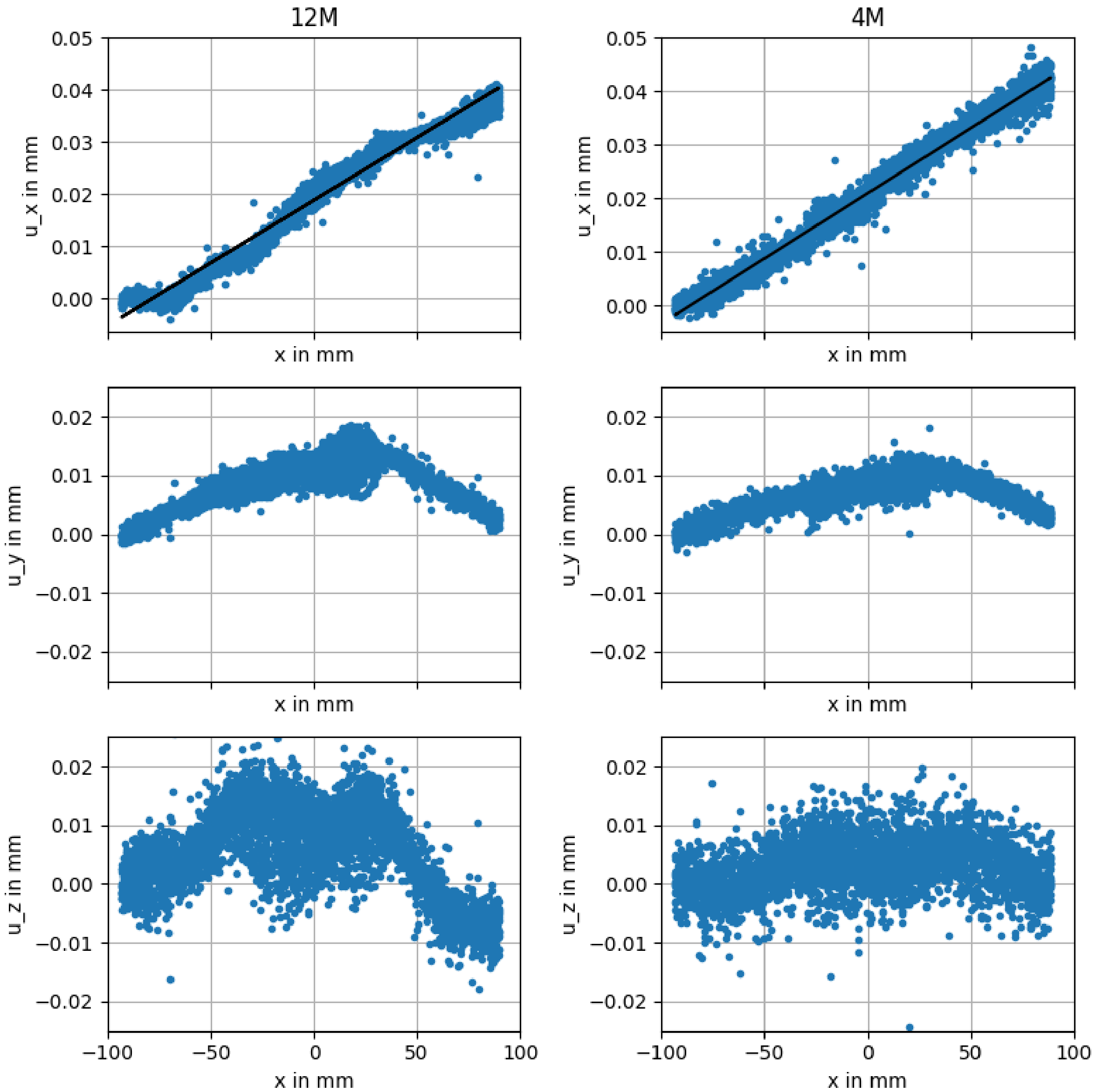

Figure 3. Filtered DIC displacements of Specimen 31 for each facet measured by both systems. The displacements are illustrated over a common global x-coordinate (along the length of the specimen) and the solid black lines are linear least squares fits to determine the stiffness reported in Table 2.

The displacements in z-direction feature significantly more noise, as the stereo DIC has a lower depth resolution than lateral resolution. Hence, we use only the in-plane displacements to compute the loss according to Equation (6) and perform 100 ADAM iterations to minimize this loss using a learning rate of 0.3 and a filter radius R=1.5mm. These parameters have proven to be suitable in a parameter study.

The resulting A_{yy} orientation (orientation perpendicular to load) for Specimen 31 is illustrated in Figure 4. The contour plots a) and c) show fiber orientations obtained by fitting the differentiable simulation to the observed linear elastic deformations. The photographs b) and d) show the specimen after fracture from the top view (as the 12M DIC system sees it) and as a center cut, respectively. The physical cut is made with a diamond band saw and allows a qualitative assessment of fiber orientations in the cutting plane. A comparison between the computed orientations and photographs indicates that the proposed method can identify a region, where many fibers are oriented perpendicular to the load direction and that this region corresponds to the location, where the specimen fails subsequently.

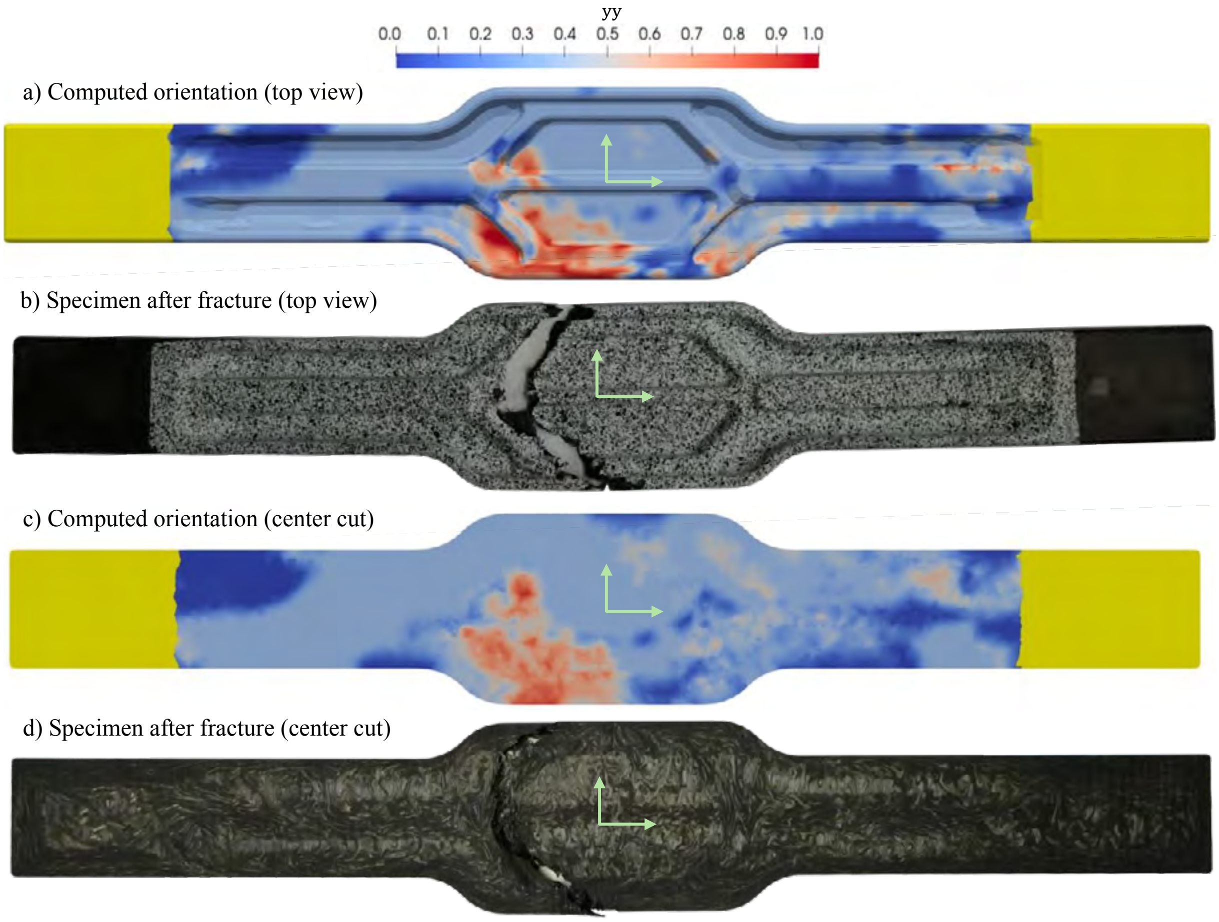

Figure 4. Computed fiber orientation tensor component A_{yy} for Specimen 31 (80% mold coverage) in comparison to photographs of the tested physical specimen.

Figure 5 shows center cut views for the remaining specimens. On average, specimens with 50% initial mold coverage feature a less prominent fiber orientation transverse to the load and a higher orientation in load direction, which agrees with the observed stiffness and the expected flow-induced reorientation. These specimens fracture close to the clamping, as indicated by the solid black lines sketching the fracture line. Specimens with 80% mold coverage feature less alignment in the load direction and have regions with fibers predominantly oriented transverse to the load direction at the specimen center. These regions correspond well with locations of subsequent fracture.

We want to highlight that the computation of orientations is based entirely on the linear elastic deformation prior to introducing any damage to the specimen. Therefore, it could be considered a non-destructive method that provides insights into the fiber orientations and potentially enables the prediction of failure.

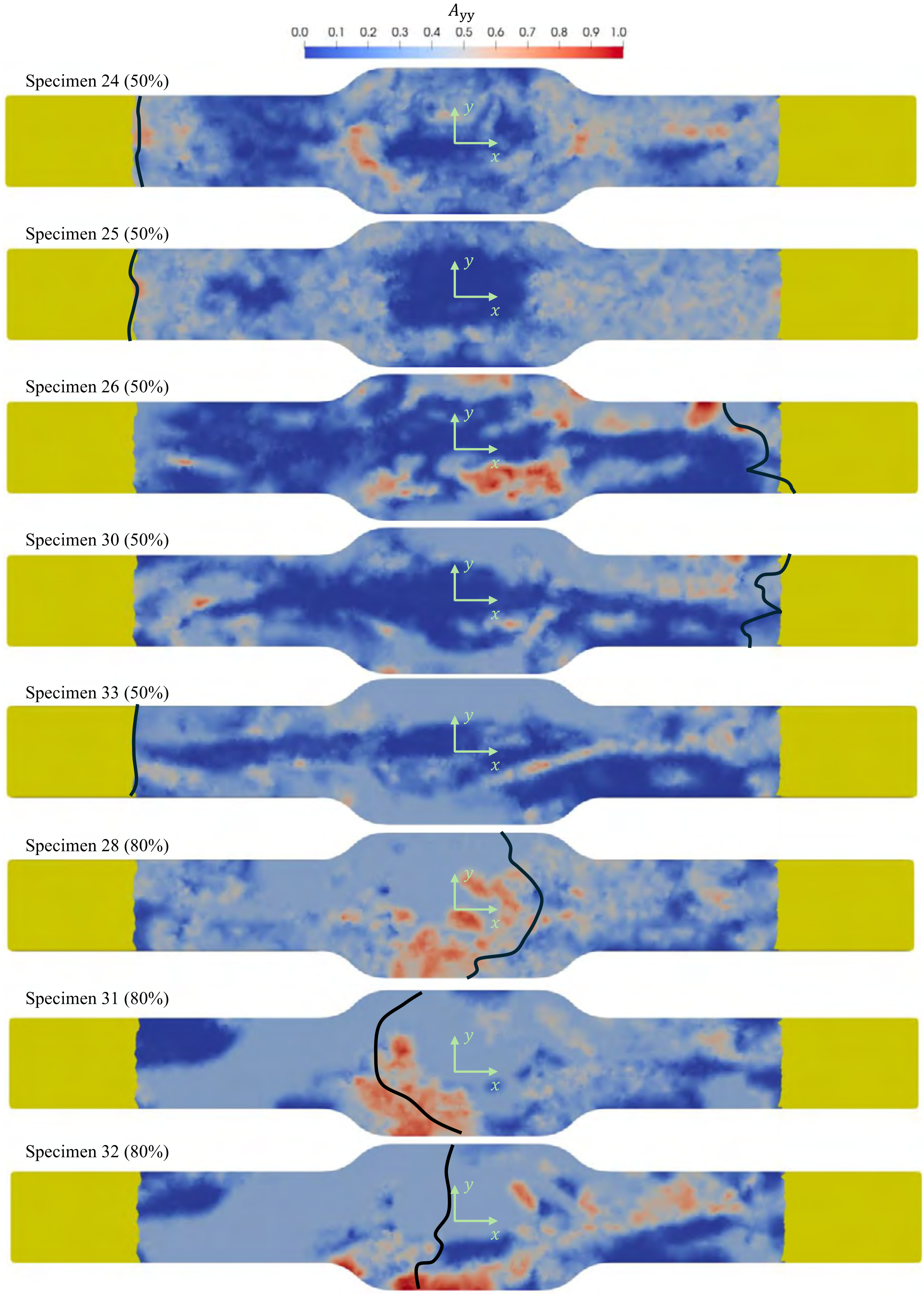

Figure 5. Computed fiber orientation tensor component A_{yy} for all specimens as center cut.

4. Conclusions and outlook

Our proposed method combines digital image correlation with differentiable finite element modeling to accurately determine local fiber orientations in polymer composite parts. We record surface displacements on two sides of CF-SMC specimens via DIC and formulate a loss term quantifying the difference between observed displacements and simulated displacements. Thanks to the fully differentiable implementation, we can efficiently minimize the loss with a gradient decent method to find orientations causing the observed deformation field. First results indicate that these orientations agree qualitatively with visual inspections of the specimens.

However, the exact orientation states vary with hyperparameters of the optimization and there is no guaranty to find a unique solution with the proposed approach. Further work is required to regularize the problem and to establish a rigorous mathematical theory on solution guarantees. In addition, misalignment or warpage of the geometry may affect the results. Analysis via µCT scans should be performed to validate the results quantitatively.

Acknowledgments

The DIC measurements were supported by Stefan Schmitt and Muhammet Bölükbas. We highly appreciate their commitment and expertise to find a suitable DIC setup. Specimen 31 was skillfully cut by Hans Eiglmeier and we thank him for his assistance at short notice.

The research documented in this manuscript has been supported by the Hightech Agenda Bavaria. The support by the Bavarian State Government is gratefully acknowledged.

References

[1] S. G. Advani and C. L. Tucker, The Use of Tensors to Describe and Predict Fiber Orientation in Short Fiber Composites, *J. Rheol.*, 31(8):751–784,1987.

[2] S. K. Kugler, A. Kech, C. Cruz, and T. Osswald, Fiber Orientation Predictions - A Review of Existing Models, *J. Compos. Sci.*, 4(2):69, 2020.

[3] N. Meyer, L. Schöttl, L. Bretz, A. N. Hrymak, and L. Kärger, Direct Bundle Simulation approach for the compression molding process of Sheet Molding Compound, *Compos. Part Appl. Sci. Manuf.*, 132:105809, 2020.

[4] M. Krause, J. M. Hausherr, B. Burgeth, C. Herrmann, and W. Krenkel, Determination of the fibre orientation in composites using the structure tensor and local X-ray transform, *J. Mater. Sci.*, 45(4):888–896, 2010.

[5] R. S. Bay and C. L. Tucker, Stereological measurement and error estimates for three-dimensional fiber orientation, *Polym. Eng. Sci.*, 32(4):240–253, 1992.

[6] D. H. Chung and T. H. Kwon, Invariant-based optimal fitting closure approximation for the numerical prediction of flow-induced fiber orientation, *J. Rheol.*, 46(1):169–194, 2002.

[7] G. P. Tandon and G. J. Weng, Average stress in the matrix and effective moduli of randomly oriented composites, *Compos. Sci. Technol.*, 27(2):111–132, 1986.

[8] N. Meyer, torch-fem, https://github.com/meyer-nils/torch-fem, accessed May 15 2024.

[9] J. K. Bauer and T. Böhlke, Variety of fiber orientation tensors, *Math. Mech. Solids*, 27(7):1185–1211, 2022.

ECCM21

02-05 July 2024 | **Nantes - France**

Volume 8

Special Sessions

ISBN: 978-2-912985-01-9
DOI: 10.60691/yj56-np80